

DART-VLN: Test-Time Memory Decay and Anti-Loop Regularization for Discrete Vision-Language Navigation

Shaoheng Zhang¹, Zhichen Li², and Jie Mei^{1,*}

¹ School of Intelligence Science and Engineering

² School of Computer Science and Technology

Harbin Institute of Technology, Shenzhen

Shenzhen, China

2023312309@stu.hit.edu.cn, 2023111963@stu.hit.edu.cn, jmei@hit.edu.cn

Abstract—Memory-based discrete vision-language navigation (VLN) agents must act under partial observability, yet even strong frozen backbones remain vulnerable at test time. Two common failure modes are stale historical evidence at memory readout and inefficient local backtracking during action selection. We present DART-VLN, a training-free test-time control framework for discrete VLN. DART-VLN combines Test-Time Memory Decay, a read-side memory reweighting rule that suppresses stale and redundant evidence without rewriting stored content, with Anti-Loop Regularization, a lightweight next-hop penalty that discourages immediate reversals during action selection. The framework introduces no new learnable parameters and leaves the learned backbone unchanged. Experiments on R2R and REVERIE show a consistent pattern: decay-only provides stable read-side gains, while decay+anti-loop achieves the best overall quality-efficiency trade-off, yielding shorter trajectories, lower runtime, and improved navigation performance in key settings. Behavioral analysis further confirms that anti-loop regularization reduces local backtracking and improves path efficiency under frozen backbones. Overall, the results show that modest test-time control can make memory-based discrete VLN more reliable and efficient without retraining.

Index Terms—Vision-Language Navigation, Discrete Navigation, Test-Time Control, Memory Decay, Anti-Loop Regularization

I. INTRODUCTION

Language-guided embodied navigation requires reliable sequential decision-making under partial observability. Vision-language navigation (VLN) provides a standard testbed for this problem by asking an embodied agent to move through an environment using language and visual observations [1], [2]. Among existing formulations, discrete VLN is especially attractive because it operates over explicit viewpoint graphs and supports controllable step-wise decision-making [3]–[5].

Recent progress in VLN has come from stronger pre-trained navigators, explicit memory or map representations, broader training resources, and more sophisticated recovery or planning mechanisms [3], [6]–[9]. Together, these advances have substantially improved long-horizon reasoning and benchmark performance. Yet a practical gap remains at inference time: even strong memory-based discrete VLN

backbones can still behave unreliably under frozen parameters. In many cases, further gains rely on retraining, architectural redesign, or heavier planning modules, which are less appealing when the goal is to strengthen an already competitive navigator with minimal intervention.

In this setting, two recurring failure modes become particularly important. The first appears at memory readout. Explicit navigation memory helps agents reason over longer trajectories by storing previously visited viewpoints, visual features, or map-level context [3]–[5], [7], [10]–[12]. Yet as navigation proceeds, stale or repeatedly observed evidence may remain active after its usefulness has faded, making memory aggregation noisier at decision time. The second appears at action selection. Even with a strong frozen backbone, agents still exhibit inefficient local behaviors such as immediate reversals and short loops [13]–[15]. These behaviors do not always destroy the final outcome, but they lengthen trajectories, waste steps, and increase runtime.

This motivates a simple question: how much can be gained from lightweight test-time control alone, without retraining the model or redesigning the navigation stack? We answer this question with DART-VLN, a training-free test-time control framework for memory-based discrete VLN. As summarized in Fig. 1, DART-VLN introduces two complementary mechanisms that operate directly inside the existing inference loop. *Test-Time Memory Decay* is a read-side reweighting rule that suppresses stale and redundant evidence during memory aggregation without rewriting stored content. *Anti-Loop Regularization* is a lightweight next-hop penalty that discourages immediate backtracking during action selection. Together, these components improve inference behavior while leaving the learned backbone untouched and introducing no new learnable parameters.

We evaluate DART-VLN on R2R and REVERIE using a GridMM-style discrete navigation pipeline [3]. The results show a consistent pattern across both benchmarks: *decay-only* isolates a stable read-side gain, while the full *decay+anti-loop* setting delivers the best overall quality-efficiency trade-off, with shorter trajectories and lower runtime under frozen backbones. Behavioral analysis further shows that the clearest direct effect of anti-loop regularization is reduced local backtracking and improved path efficiency. These findings suggest that modest test-time control

* Corresponding author.

Code will be released at <https://github.com/Japluto/DART-VLN>.

Overview of DART-VLN as a training-free test-time control framework for discrete vision-language navigation

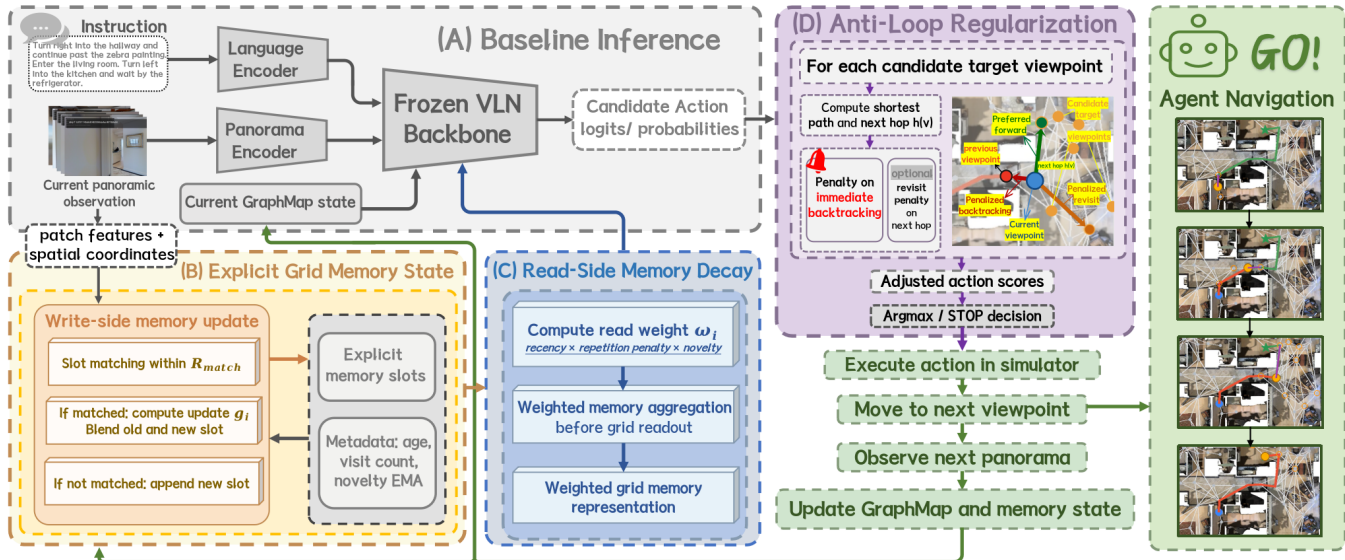


Fig. 1. DART-VLN test-time pipeline for discrete VLN. The environment maintains explicit grid memory with optional write-side updates (update-only/full-mode). Read-side memory decay reweights memory during grid aggregation, and anti-loop regularization adjusts candidate action scores using next-hop penalties before argmax. No retraining or new learnable parameters are introduced.

can meaningfully strengthen memory-based discrete VLN without reopening training.

A. Contributions

- We propose a training-free read-side memory control strategy that suppresses stale and redundant historical evidence during memory readout without rewriting stored memory content.
- We propose a lightweight next-hop-based action regularization mechanism that reduces local backtracking and improves efficiency-side trajectory behavior during inference.
- Experiments on representative discrete VLN benchmarks show that *decay-only* isolates a stable read-side gain, while the full *decay+anti-loop* setting achieves the most favorable quality-efficiency trade-off under frozen backbones.

II. RELATED WORK

Memory and map-based discrete VLN: Explicit memory and map representations have become a common way to stabilize long-horizon reasoning in discrete VLN. Recent methods store visited viewpoints, aggregate graph-level context, or build richer topological or map-like state representations for navigation [3]–[5], [10], [11]. Although these approaches differ in form, they share a common goal: strengthening spatial grounding and history aggregation through a more informative external state. By contrast, DART-VLN does not introduce a new memory structure, map encoder, or fusion architecture. Instead, it operates on top of an existing explicit-memory pipeline and focuses on improving how historical evidence is used at test time under frozen parameters. The distinction is therefore not whether memory matters, but

whether improvement comes from richer memory construction or from tighter control over memory usage at inference time.

Backtracking, rewind, and local recovery: A second line of work targets local navigation failures such as wrong turns, backtracking, and short loops [13]–[15]. Regret-aware and foresighted navigation methods show that local recovery decisions can materially affect trajectory efficiency, while more planning-oriented approaches further strengthen correction behavior through richer control mechanisms. These methods highlight the importance of local trajectory management, but they are often coupled with learned progress estimation, explicit correction policies, or stronger planning modules. Our anti-loop module shares the same behavioral motivation, yet it is deliberately narrower in scope: it acts as a lightweight next-hop regularizer on graph-local action scores at inference time, rather than as a planner or learned self-correction policy.

Inference-time control versus retraining-heavy improvement: Many strong gains in VLN come from architectural extension, richer scene modeling, or heavier planning modules [8], [9], [16]. These directions are effective, but they are less suitable when the practical goal is to improve an already competitive frozen navigator without reopening the training pipeline. More recent work has also begun exploring training-free or test-time intervention in VLN, reflecting growing interest in improving deployed navigators without a new training cycle [17], [18]. DART-VLN is positioned in this low-intrusion regime: it introduces no new learnable parameters, leaves the learned backbone unchanged, and confines intervention to read-side memory control and action-side local regularization. In this sense, our goal is not to redesign the navigator itself, but to improve its test-time behavior in a lightweight and interpretable manner.

III. METHOD

A. Problem Setting and Baseline Navigation Inference

We consider a memory-based agent operating on a discrete navigation graph $G = (V, E)$, where each node denotes a viewpoint and each edge represents a feasible transition. Given a natural-language instruction x , the agent starts from an initial viewpoint v_0 and makes sequential navigation decisions over the graph, producing a trajectory $\tau = (v_0, v_1, \dots, v_T)$. At each step t , the agent receives the current visual observation at v_t , retrieves historical information from an explicit navigation memory, and scores the candidate actions reachable from the current viewpoint.

Our method is built on a GridMM-style discrete VLN pipeline [3]. The baseline encodes the instruction and current observation, aggregates historical evidence from explicit memory slots $\{m_i\}$, and computes action scores $s_t(v)$ for candidate target viewpoints v before selecting the next action. This explicit-memory design provides useful long-horizon context, but it also introduces an inference-time challenge: historical evidence that is stale or repeatedly observed may continue to influence the current decision.

Our goal is not to redesign the backbone, memory structure, or training objective. Instead, we introduce lightweight test-time control into the existing inference loop. Specifically, we intervene at memory readout and action selection: memory slots are reweighted during aggregation to suppress stale or redundant evidence, and candidate scores are regularized before argmax decoding to discourage inefficient local reversals. Throughout this process, the learned backbone remains frozen and no new learnable parameters are introduced.

Although motivated by reliable embodied navigation under partial observability [19], the method is defined and validated here in a representative discrete VLN setting. The following subsections describe the proposed read-side memory control and action-side regularization in detail.

B. Test-Time Memory Decay

1) *Motivation*: In memory-based navigation, not all historical evidence remains equally useful throughout inference [10], [11], [16]. As the trajectory grows, some memory slots may encode information that is outdated, overly repeated, or only weakly relevant to the current decision. If such evidence continues to contribute with the same strength as fresher observations, memory aggregation can become noisier and less selective at test time.

To address this issue, we adopt a conservative read-side strategy. Rather than rewriting stored memory content, we adjust only how strongly each slot contributes at readout. This preserves compatibility with the baseline memory structure while allowing stale and redundant evidence to be suppressed during inference.

2) *Slot Metadata*: For each memory slot m_i , we maintain three lightweight metadata variables: slot age a_i , visit count c_i , and novelty n_i . The slot age is defined as

$$a_i = t - t_i^{\text{last}},$$

where t_i^{last} is the most recent step at which slot i was refreshed. The visit count c_i reflects how often the corresponding region has been repeatedly observed. The novelty term n_i captures recent feature change and is smoothed over time.

Concretely, let f_i^{old} and f_i^{new} denote the previous and current slot features. We first compute an instantaneous novelty score

$$\nu_i = \text{clip}(1 - \cos(f_i^{\text{old}}, f_i^{\text{new}}), 0, 1), \quad (1)$$

and then update the novelty estimate with an exponential moving average:

$$n_i^{(t)} = \rho n_i^{(t-1)} + (1 - \rho)\nu_i. \quad (2)$$

Here, $\rho \in [0, 1)$ controls how strongly past novelty estimates are retained over time. In our implementation, $\rho = 0.5$. Together, these metadata provide a lightweight summary of whether a slot is recent, over-repeated, or still changing in a potentially useful way.

3) *Memory Reweighting*: Based on the metadata above, we assign a heuristic readout weight w_i to each memory slot. Since ν_i is clipped to $[0, 1]$ and n_i is obtained by exponential smoothing, we also have $n_i \in [0, 1]$. The readout weight is defined as

$$w_i = \text{clip}\left(\exp(-\lambda a_i) \left(1 - \alpha \frac{c_i}{c_i + 1}\right) (0.5 + 0.5 n_i), w_{\min}, w_{\max}\right). \quad (3)$$

This formulation combines three intuitive factors. The recency term $\exp(-\lambda a_i)$ downweights slots that have not been refreshed for many steps. The repetition term $(1 - \alpha \frac{c_i}{c_i + 1})$ reduces the influence of slots associated with repeatedly observed regions, where α controls the strength of repetition suppression. The novelty term $(0.5 + 0.5 n_i)$ softly favors slots that still exhibit noticeable recent feature change. Finally, clipping to $[w_{\min}, w_{\max}]$ prevents the reweighting from becoming either too weak or too aggressive.

In the main design, these weights are applied only during memory readout. The weighted memory is then passed into the original navigation pipeline without modifying the stored slot content itself. This keeps the intervention simple, training-free, and easy to isolate in ablation.

4) *Boundary of Decay-Only*: In the *decay-only* setting, only the read-side reweighting in Eq. (3) is applied. The stored slot representation and the baseline memory update behavior remain unchanged. This distinguishes the method from write-side heuristics that directly rewrite memory content. In other words, *decay-only* should be viewed as a read-side denoising rule rather than as a new memory-learning mechanism.

5) *Write-Side Memory Update Variants*: Beyond read-side decay, we also explored a more aggressive write-side memory update before readout. In this exploratory setting, matched slots are refreshed with a simple heuristic gate based on novelty, age, and repetition statistics, while unmatched observations append new slots. We report the write-side

update alone as *update-only* and its combination with read-side decay as *full-mode*. Because these rewriting variants were less stable than the conservative read-side design, we treat them as boundary comparisons rather than as part of the DART-VLN mainline.

C. Anti-Loop Regularization for Navigation Decision-Making

1) *Motivation*: Immediate backtracking is a common local failure mode in embodied navigation [13]–[15]. Repeated reversals and related short loops can inflate path length, waste steps, and degrade trajectory efficiency even when the agent eventually reaches a reasonable destination. These behaviors therefore matter not only because they are inefficient, but also because they expose the agent to additional decision points that may accumulate further error at test time.

This makes local loop suppression a suitable target for lightweight inference-time control. In our design, anti-loop regularization is intentionally conservative: its purpose is to improve local path behavior under frozen backbones, rather than to serve as a planner or to guarantee monotonic gains on all endpoint metrics.

2) *Next-Hop Based Penalty*: Let $s_t(v)$ denote the original action score assigned at step t to a candidate target viewpoint v . Rather than directly penalizing a final candidate viewpoint, we examine the graph next hop $h(v)$, namely the first local transition on the path from the current viewpoint to v . We then define a lightweight penalty

$$p_t(v) = \beta_{\text{back}} \cdot \mathbb{I}[h(v) = v_{t-1}] + \beta_{\text{rev}} \cdot \mathbb{I}[\text{visit}(h(v)) \geq k], \quad (4)$$

and use it to adjust the action score:

$$s'_t(v) = s_t(v) - p_t(v). \quad (5)$$

The first term penalizes immediate backtracking, i.e., cases where the next hop directly returns to the previous viewpoint v_{t-1} . The second term provides a weak extension for repeated revisits. Here, $\text{visit}(h(v))$ denotes the number of prior visits to the next-hop viewpoint, β_{rev} controls the revisit penalty strength, and k is the revisit threshold. In the finalized setting, this revisit term is kept small and activated only after repeated revisits with $k = 2$. As a result, the dominant effect of the module remains immediate backtrack suppression.

This next-hop formulation is important because it targets the local transition actually executed at the current step, rather than only adjusting a more distant target score. It therefore aligns the regularizer with the trajectory-level behavior we aim to change.

3) *Inference Scope*: The anti-loop module is applied only at test time and is intended for deterministic, argmax-based navigation inference. In the full DART-VLN configuration, it is combined with read-side memory decay and applied to candidate action scores before action selection. The module does not modify the stop head, introduce a separate planning component, or alter the learned backbone. Its scope is deliberately narrow: it acts as a graph-local action regularizer for improving efficiency-side behavior under frozen inference.

Algorithm 1: Mainline DART-VLN Inference

Notation: $h(v)$: graph next hop of candidate viewpoint v
 $p_t(v)$: anti-loop penalty
 $s'_t(v)$: adjusted action score
Input : Instruction x ; initial viewpoint v_0 ; max step T_{max} ; memory slots $\{m_i\}$ with metadata $\{a_i, c_i, n_i\}$
Output : Navigation trajectory τ

```

1 Function DART-VLN-Infer( $x, v_0, \{m_i, a_i, c_i, n_i\}, T_{\text{max}}$ ):
2   Initialize  $\tau \leftarrow (v_0)$  and the visit counts from the start
   viewpoint
3   for  $t \leftarrow 0$  to  $T_{\text{max}} - 1$  do
4     Encode the instruction and current observation at  $v_t$ 
5     Compute read-side memory weights  $w_i$  using Eq. (3)
6     Aggregate weighted memory and obtain candidate scores
      $\{s_t(v)\}$ 
7     for each candidate target viewpoint  $v$  do
8       Compute graph next hop  $h(v)$  from the current
       viewpoint
9       Compute penalty  $p_t(v)$  using Eq. (4)
10      Update adjusted score  $s'_t(v) \leftarrow s_t(v) - p_t(v)$ 
11      Select the next action by  $\arg \max_v s'_t(v)$ 
12      if STOP is selected then
13        return  $\tau$ 
14      Execute the transition and append the new viewpoint to  $\tau$ 
15      Update visit counts and refresh memory / slot metadata
     for the next step
16  return  $\tau$ 

```

D. Design Principle: Conservative Test-Time Control

DART-VLN follows a simple principle: under frozen backbones, modest test-time interventions are often more dependable than aggressive rewriting or correction. Accordingly, the practical mainline combines read-side memory decay with local anti-loop regularization, rather than relying on heavier manipulation of the navigation process.

This choice is intentional. Read-side reweighting suppresses stale evidence without perturbing the stored representation used by the backbone, while the action-side regularizer is kept narrow so that it discourages wasteful local loops without over-constraining exploration. For this reason, more aggressive variants are treated only as boundary comparisons rather than as part of the final method. Algorithm 1 summarizes the resulting inference flow.

IV. EXPERIMENTS

A. Experimental Setup

We evaluate DART-VLN on two representative discrete VLN benchmarks: Room-to-Room (R2R) [1] and REVERIE [20]. There are several standard metrics for evaluating VLN agents, including Trajectory Length (TL), Navigation Error (NE), Success Rate (SR), Oracle Success Rate (OSR), Success weighted by Path Length (SPL), Remote Grounding Success (RGS), and Remote Grounding Success weighted by Path Length (RGSPL). For R2R, Table I reports TL, NE, SR, SPL, and runtime on *val unseen* and *test unseen*. For REVERIE, Table II reports TL, OSR, SR, SPL, RGS, RGSPL, and runtime on *val unseen*. In the discussion below, we mainly treat SR, SPL, and RGSPL as the primary task metrics, while TL, NE, and runtime are used to interpret efficiency and stability under frozen backbones.

All variants use the same checkpoints as the baseline and differ only in inference-time control switches; no retraining is involved. Unless otherwise stated, DART-VLN refers to

TABLE I
RESULTS ON THE R2R DATASET

Methods	Val Unseen					Test Unseen				
	TL↓	NE↓	SR↑	SPL↑	Runtime(s)↓	TL↓	NE↓	SR↑	SPL↑	Runtime(s)↓
VLNBERT [6]	12.03	3.93	63	57	–	12.37	4.11	63	57	–
AirBERT [21]	11.78	3.99	62	56	–	12.40	4.15	62	57	–
SEvol [9]	12.22	3.96	62	57	–	13.42	4.17	62	57	–
HOP [22]	12.28	3.81	64	57	–	12.71	3.87	64	59	–
HAMT [7]	11.44	2.31	66	61	–	12.27	3.95	65	60	–
TD-STP [23]	–	3.23	70	63	–	–	3.72	67	61	–
DUET [4]	13.92	3.33	72	60	–	14.71	3.63	69	59	–
BEVBert [5]	14.52	2.83	74	64	–	15.88	3.15	73	62	–
GridMM (baseline) [3]	13.27	2.83	74	64	937.99	14.43	3.35	73	62	2312.52
update-only	13.92	2.86	75	63	891.12	16.2	3.37	72	59	1725.22
decay-only	13.29	2.59	76	65	742.61	14.52	3.19	73	62	1621.34
full-mode	13.77	2.80	75	64	1000.84	15.95	3.30	72	60	2475.63
decay+anti-loop	12.41↓	2.69	76↑	66↑	666.37↓	13.80↓	3.38	74↑	63↑	1329.56↓

Note: GridMM is the baseline of our experiments. Runtime is reported only for GridMM and its inference-time variants, because **runtime comparisons across papers are not directly meaningful and depend on implementation details, hardware, simulator settings, and backbone scale.**

the combined *decay+anti-loop* configuration under deterministic argmax inference. We also report *update-only*, *decay-only*, and *full-mode* as ablation and boundary variants. The mainline setting uses $\lambda = 0.12$, $\alpha = 0.15$, $w_{\min} = 0.35$, $w_{\max} = 1.0$, $\beta_{\text{back}} = 0.22$, $\beta_{\text{rev}} = 0.06$, and $k = 2$. For the exploratory write-side variants, we use $g_0 = 0.15$, $\lambda_n = 0.35$, $\lambda_a = 0.20$, $\lambda_c = 0.15$, $g_{\min} = 0.05$, $g_{\max} = 0.85$, $T_{\max} = 20$, and $r_{\text{match}} = 0.75$. Runtime is reported only for GridMM and its inference-time variants. Cross-paper runtime is not directly comparable because it depends on implementation details, hardware, simulator settings, and backbone scale. All runtime measurements in this work are obtained under the same implementation and hardware setting on an NVIDIA GeForce RTX 5070 Ti GPU. For the behavioral diagnosis in Table III, backtrack rate is defined as the percentage of executed actions whose next viewpoint returns to the viewpoint from two steps earlier, and Avg. Steps counts actions before STOP.

B. Main Results on R2R and REVERIE

Tables I and II summarize the main results on R2R and REVERIE, respectively. Across both benchmarks, the same broad trend appears: *decay-only* already yields a clear read-side gain over the GridMM baseline, while the full *decay+anti-loop* configuration provides the strongest overall quality-efficiency trade-off. We discuss the benchmark-specific outcomes below and return to the role of the boundary variants in Sec. IV-C.

R2R. Table I reports results on both *val unseen* and *test unseen*. On this benchmark, *decay-only* already shows the value of conservative read-side control: compared with GridMM, it improves NE from 2.83 to 2.59 on *val unseen* and from 3.35 to 3.19 on *test unseen*, while also reducing runtime from 937.99s to 742.61s and from 2312.52s to 1621.34s, respectively. Its SR and SPL are maintained or slightly improved, which suggests that suppressing stale and redundant evidence at memory readout can make the baseline inference process both cleaner and more efficient.

Adding anti-loop regularization yields the best overall variant on R2R. The *decay+anti-loop* setting achieves the

TABLE II
RESULTS ON REVERIE VAL UNSEEN DATASET

Methods	Val Unseen						Runtime(s)↓
	Navigation			Grounding			
	TL↓	OSR↑	SR↑	SPL↑	RGS↑	RG SPL↑	
VLNBERT [6]	16.75	35.08	30.63	24.90	18.72	15.23	–
AirBERT [21]	18.71	34.51	27.88	21.83	18.19	14.16	–
HOP [22]	16.46	36.24	31.78	26.15	18.82	15.73	–
HAMT [7]	14.08	36.84	32.91	30.23	18.90	17.26	–
TD-STP [23]	–	39.48	34.89	27.34	21.13	16.52	–
DUET [4]	22.12	51.08	46.96	33.77	32.12	23.01	–
BEVBert [5]	–	56.38	51.79	36.35	34.70	24.46	–
GridMM [3]	23.20	57.48	51.37	36.47	34.57	24.56	4329.67
update-only	23.77	57.12	50.84	35.85	33.98	23.80	4276.31
decay-only	23.15	58.12	51.98	36.60	34.68	24.72	2998.49
full-mode	23.18	57.94	51.80	36.45	34.65	24.68	4603.40
decay+anti-loop	21.57	57.99	52.34	37.53	35.37	25.44	1497.98

Note: GridMM is the baseline of our experiments. Runtime is reported only for GridMM and its inference-time variants, because **runtime comparisons across papers are not directly meaningful and depend on implementation details, hardware, simulator settings, and backbone scale.** The official REVERIE test unseen evaluation server is no longer available, so we report only Val Unseen results.

shortest trajectory length and the lowest runtime on both splits, while also improving SR and SPL over the baseline. On *val unseen*, it reduces TL from 13.27 to 12.41 and raises SPL from 64 to 66. On *test unseen*, it reduces TL from 14.43 to 13.80 and improves SR/SPL from 73/62 to 74/63. Although NE on *test unseen* does not improve monotonically relative to the baseline (3.38 versus 3.35), the overall result still reflects the most favorable balance between navigation quality and execution efficiency.

REVERIE. Table II reports results on *val unseen*, which remains the most relevant split for unseen generalization in the currently available evaluation setting. REVERIE shows the same qualitative trend as R2R. The *decay-only* variant again provides a clean conservative gain: relative to GridMM, it slightly improves OSR, SR, SPL, RGS, and RG SPL, while reducing runtime from 4329.67s to 2998.49s. This indicates that the benefit of read-side memory control is not limited to standard navigation success, but also transfers to the more demanding setting where remote object grounding is part of the task outcome.

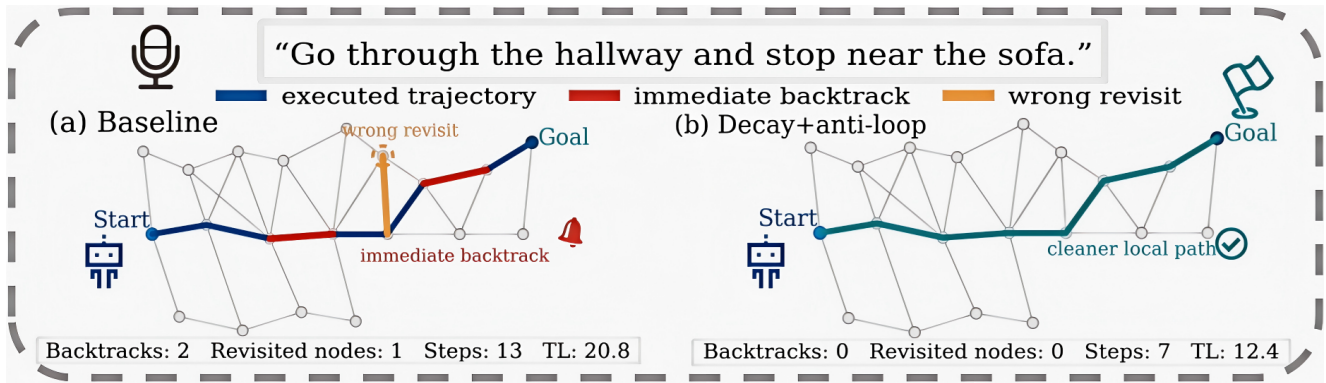


Fig. 2. Qualitative local behavior under anti-loop regularization. Compared with the baseline, *decay+anti-loop* avoids immediate backtracking and wrong revisits, yielding a shorter local path.

The full *decay+anti-loop* configuration provides the strongest overall result on REVERIE. Compared with GridMM, it shortens TL from 23.20 to 21.57, improves SR from 51.37 to 52.34, raises SPL from 36.47 to 37.53, and increases RGSPL from 24.56 to 25.44. The runtime reduction is especially notable, dropping from 4329.67 s to 1497.98 s. As on R2R, this pattern suggests that anti-loop regularization is most valuable when added on top of the more stable read-side decay variant, rather than when paired with stronger write-side intervention.

Taken together, the two benchmarks support the same practical conclusion: read-side decay provides a stable improvement over the baseline, and adding anti-loop regularization further strengthens the overall quality-efficiency trade-off. The next subsection examines the role of the remaining variants more directly.

C. Ablation and Boundary Variants

The comparison among *update-only*, *decay-only*, *full-mode*, and *decay+anti-loop* helps clarify the role of each component in DART-VLN. The first observation is that *decay-only* provides the most stable single-module gain. Across both R2R and REVERIE, it consistently improves or preserves the main task metrics while reducing runtime relative to the GridMM baseline. This supports our central claim that lightweight read-side memory control alone can already improve frozen-backbone inference without modifying the stored memory representation.

The second observation is that stronger intervention is not necessarily better. Both *update-only* and *full-mode* introduce write-side memory rewriting before readout, making them more aggressive than the conservative read-side design. However, their gains are less consistent across benchmarks and, in several cases, they underperform both *decay-only* and the final *decay+anti-loop* configuration. This suggests that under frozen backbones, directly rewriting stored memory may disturb representations that the baseline policy already uses effectively. For this reason, we treat these variants as boundary comparisons rather than as part of the DART-VLN mainline.

The third observation is that *decay+anti-loop* should be interpreted as building on the stable read-side gain of *decay-only*, rather than replacing it. The consistent pattern across

Tables I and II is that memory decay provides the stronger and more dependable base improvement, while anti-loop regularization adds a narrow action-side controller that further improves the practical quality-efficiency trade-off. In this sense, the final method is not defined by maximal intervention, but by the most reliable combination under frozen inference. The overall ablation therefore supports the design principle of DART-VLN: under frozen backbones, modest and well-scoped test-time control is more reliable than heavier intervention.

D. Navigation Behavior and Efficiency Analysis

We do not position anti-loop regularization as a mechanism that guarantees monotonic gains on all final navigation metrics. Instead, its most direct value lies in improving local trajectory behavior under frozen backbones. Figure 2 provides an illustrative example, while Table III quantifies the same pattern through immediate backtrack rate, average action steps, and average trajectory length.

On R2R, the comparison among the baseline, *decay-only*, and *decay+anti-loop* makes this distinction clear. The *decay-only* variant leaves local reversal behavior essentially unresolved: its average action count changes only marginally, and its immediate backtrack rate is slightly higher than that of the baseline. This is consistent with its role as a read-side denoising rule rather than a direct motion regularizer. By contrast, adding anti-loop regularization lowers the immediate backtrack rate from 3.51% to 2.01%, while further reducing average action steps and trajectory length. In other words, the action-side controller does not merely change final scores; it changes how the trajectory is executed.

The same interpretation is supported on REVERIE. Here, the baseline and *decay-only* remain nearly identical in local reversal behavior, whereas *decay+anti-loop* lowers the immediate backtrack rate from 8.45% to 5.99% and further shortens the executed trajectory. The directional consistency across R2R and REVERIE is important: although the two benchmarks emphasize different endpoint outcomes, the proposed regularizer alters graph-local behavior in the same way on both of them.

This result matters from a practical inference perspective. Wasteful reversals consume extra actions, increase runtime,

TABLE III

BEHAVIORAL DIAGNOSIS ON R2R AND REVERIE VAL UNSEEN.

Methods	R2R Val Unseen		
	Backtrack Rate(%)↓	Avg. Steps↓	Avg. TL↓
GridMM (baseline)	2.30	6.02	13.27
decay-only	3.51	6.00	13.29
decay+anti-loop	2.01↓	5.90↓	12.41↓
Methods	REVERIE Val Unseen		
	Backtrack Rate(%)↓	Avg. Steps↓	Avg. TL↓
GridMM (baseline)	8.43	8.52	23.18
decay-only	8.45	8.52	23.15
decay+anti-loop	5.99↓	8.46↓	21.57↓

Note: Backtrack rate is the percentage of executed actions that return to the viewpoint from two steps earlier; Avg. Steps counts actions before STOP. The mainline uses only a weak revisit term, so the observed changes are still dominated by immediate backtrack suppression.

and expose the agent to more decision points without necessarily adding useful evidence. Reducing such oscillatory transitions therefore improves not only efficiency, but also the interpretability of the executed path. In this sense, the value of anti-loop regularization is best understood as a conservative local controller that makes frozen-backbone inference cleaner and more efficient, rather than as a standalone explanation for every endpoint gain.

V. CONCLUSION

This paper studied how to strengthen memory-based discrete VLN under frozen backbones through lightweight test-time control. DART-VLN combines read-side memory decay with action-side anti-loop regularization, improving the practical quality-efficiency trade-off without retraining or architectural redesign. Across R2R and REVERIE, the method shows a consistent pattern: *decay-only* provides a stable read-side gain, while the final *decay+anti-loop* configuration yields the best overall balance of navigation quality, trajectory efficiency, and runtime. Behavioral analysis further shows that the clearest direct effect of anti-loop regularization is reduced local backtracking and cleaner path execution under frozen inference.

These findings should be interpreted within scope. The current study is centered on discrete VLN benchmarks with a GridMM-style backbone, and the most direct evidence for anti-loop regularization lies in local behavior and efficiency rather than in a complete causal explanation of every endpoint gain. Even with these limits, the practical message is clear: when a strong memory-based navigator is already available, modest and interpretable test-time control can still improve inference behavior without reopening training. Extending this perspective to other backbones and broader embodied navigation settings is a natural direction for future work.

REFERENCES

[1] P. Anderson, Q. Wu, D. Teney, J. Bruce, M. Johnson, N. Sünderhauf, I. Reid, S. Gould, and A. van den Hengel, "Vision-and-language navigation: Interpreting visually-grounded navigation instructions in real environments," in *Proc. IEEE/CVF Conf. Comput. Vis. Pattern Recognit.*, 2018, pp. 3674–3683.

[2] Y. Zhang, Z. Ma, J. Li, Y. Qiao, Z. Wang, J. Chai, Q. Wu, M. Bansal, and P. Kordjamshidi, "Vision-and-language navigation today and tomorrow: A survey in the era of foundation models," *Trans. Mach. Learn. Res.*, 2024.

[3] Z. Wang, X. Li, J. Yang, Y. Liu, and S. Jiang, "GridMM: Grid memory map for vision-and-language navigation," in *Proc. IEEE/CVF Int. Conf. Comput. Vis.*, 2023, pp. 15 579–15 590.

[4] S. Chen, P.-L. Guhur, M. Tapaswi, C. Schmid, and I. Laptev, "Think global, act local: Dual-scale graph transformer for vision-and-language navigation," in *Proc. IEEE/CVF Conf. Comput. Vis. Pattern Recognit.*, 2022, pp. 16 537–16 547.

[5] D. An, Y. Qi, Y. Li, Y. Huang, L. Wang, T. Tan, and J. Shao, "BEVBert: Topo-metric map pre-training for language-guided navigation," *arXiv:2212.04385*, 2022.

[6] Y. Hong, Q. Wu, Y. Qi, C. Rodriguez-Opazo, and S. Gould, "VLN-BERT: A recurrent vision-and-language BERT for navigation," in *Proc. IEEE/CVF Conf. Comput. Vis. Pattern Recognit.*, 2021, pp. 1643–1653.

[7] S. Chen, P.-L. Guhur, C. Schmid, and I. Laptev, "History aware multimodal transformer for vision-and-language navigation," in *Adv. Neural Inf. Process. Syst.*, 2021.

[8] C. Gao, X. Peng, M. Yan, H. Wang, L. Yang, H. Ren, H. Li, and S. Liu, "Adaptive zone-aware hierarchical planner for vision-language navigation," in *Proc. IEEE/CVF Conf. Comput. Vis. Pattern Recognit.*, 2023, pp. 14 911–14 920.

[9] X. Dong, H. Zhao, J. Gao, H. Li, X. Ma, Y. Zhou, F. Chen, and J. Liu, "SE-VLN: A self-evolving vision-language navigation framework based on multimodal large language models," *arXiv:2507.13152*, 2025.

[10] J. Gao, R. Liu, and W. Wang, "3D Gaussian map with open-set semantic grouping for vision-and-language navigation," in *Proc. IEEE/CVF Int. Conf. Comput. Vis.*, 2025, pp. 9252–9262.

[11] S. Zhang, Y. Qiao, Q. Wang, Z. Yan, Q. Wu, Z. Wei, and J. Liu, "COSMO: Combination of selective memorization for low-cost vision-and-language navigation," in *Proc. IEEE/CVF Int. Conf. Comput. Vis.*, 2025, pp. 5511–5522.

[12] J. Krantz, S. Banerjee, W. Zhu, J. Corso, P. Anderson, S. Lee, and J. Thomason, "Iterative vision-and-language navigation," in *Proc. IEEE/CVF Conf. Comput. Vis. Pattern Recognit.*, 2023, pp. 14 921–14 930.

[13] C.-Y. Ma, Z. Wu, G. AlRegib, C. Xiong, and Z. Kira, "The regretful agent: Heuristic-aided navigation through progress estimation," in *Proc. IEEE/CVF Conf. Comput. Vis. Pattern Recognit.*, 2019, pp. 6732–6740.

[14] H. Wang, W. Liang, L. Van Gool, and W. Wang, "DREAMWALKER: Mental planning for continuous vision-language navigation," in *Proc. IEEE/CVF Int. Conf. Comput. Vis.*, 2023, pp. 10 839–10 849.

[15] P. Xu, X. Gong, and Y. Mu, "NavQ: Learning a Q-model for foresighted vision-and-language navigation," in *Proc. IEEE/CVF Int. Conf. Comput. Vis.*, 2025, pp. 6327–6341.

[16] G. Georgakis, K. Schmeckpeper, K. Wanchoo, S. Dan, E. Mitsakaki, D. Roth, and K. Daniilidis, "Cross-modal map learning for vision and language navigation," in *Proc. IEEE/CVF Conf. Comput. Vis. Pattern Recognit.*, 2022, pp. 15 460–15 470.

[17] N. Rajabi and J. Kosecka, "TRAVEL: Training-free retrieval and alignment for vision-and-language navigation," *arXiv:2502.07306*, 2025.

[18] H. Ko, S. Kim, G. Oh, J. Yoon, H. Lee, S. Jang, S. Kim, and S. Kim, "Active test-time vision-language navigation," in *Adv. Neural Inf. Process. Syst.*, 2025.

[19] J. Krantz, E. Wijmans, A. Majumdar, D. Batra, and S. Lee, "Beyond the nav-graph: Vision-and-language navigation in continuous environments," in *Proc. Eur. Conf. Comput. Vis.*, 2020, pp. 104–120.

[20] Y. Qi, Q. Wu, P. Anderson, X. Wang, W. Y. Wang, C. Shen, and A. van den Hengel, "REVERIE: Remote embodied visual referring expression in real indoor environments," in *Proc. IEEE/CVF Conf. Comput. Vis. Pattern Recognit.*, 2020, pp. 9979–9988.

[21] P.-L. Guhur, M. Tapaswi, H. Chen, I. Laptev, and C. Schmid, "Airtbert: In-domain pretraining for vision-and-language navigation," in *Proc. IEEE/CVF Int. Conf. Comput. Vis.*, 2021, pp. 1614–1623.

[22] Y. Qiao, Y. Qi, Y. Hong, Z. Yu, P. Wang, and Q. Wu, "HOP+: History-enhanced and order-aware pre-training for vision-and-language navigation," *IEEE Trans. Pattern Anal. Mach. Intell.*, vol. 45, no. 7, pp. 8524–8537, 2023.

[23] Y. Zhao, J. Chen, C. Gao, W. Wang, L. Yang, H. Ren, H. Xia, and S. Liu, "Target-driven structured transformer planner for vision-language navigation," in *Proc. 30th ACM Int. Conf. Multimedia*, 2022, pp. 4194–4203.